PHASE EQUILIBRIA IN THE Cu_2Se - Cu_3SbSe_4 - Cu_2SnSe_3 SYSTEM

E.N. Ismailova, L.F. Mashadieva, I.B. Bakhtiyarly, V.A. Gasymov, R.J. Gurbanova, F.M. Mammadova

Institute of Catalysis and Inorganic Chemistry n.a. M. Nagiyev
Az1143, 113 H. Javid ave., Baku, Azerbaijan
e-mail: Ismayilova818@mail.ru

Received 31.07.2024
Accepted 19.09.2024

Abstract: *Copper-tin and copper-antimony chalcogenides have received increasing attention as promising thermoelectric materials due to their high efficiency and low toxicity. Many of these phases are synthetic analogues of natural copper chalcogenide minerals and have been drawing more interest for the development of new environmentally friendly materials. In this regarding, we studied phase equilibria in the Cu_2Se - Cu_3SbSe_4 - Cu_2SnSe_3 system using Differential Thermal Analysis (DTA), Powder x-ray Diffraction (PXRD) and Scanning Electron Microscope (SEM). Based on experimental data, a number of polythermal sections, the solid-phase equilibria diagram at 600 K and a projection of the liquidus surface were constructed for the title system. The system has revealed limited regions of solid solutions based on ternary compounds Cu_3SbSe_4 (α) and Cu_2SnSe_3 (β). It has been established that the liquidus surface consists of three regions corresponding to primary crystallization (HT-Cu_2Se), as well as α- and β-phases.*
Keywords*: phase diagram, liquidus surface, copper-tin-antimony selenides, and solid solutions.*
DOI: 10.32737/2221-8688-2025-1-36-46

1. Introduction

Ternary and complex copper chalcogenides have been the subject of extensive research due to their many applications, including thermoelectric (TE) and photoelectric capabilities, among others [1–9]. Some of them are attractive materials with considerable potentials to achieve improved TE performance with various cationic and anionic substitutions [10-13]. Particularly, compounds and phases of variable composition of the Cu-Sn-Sb-X (X= S, Se) systems illustrated highly effective thermoelectric properties in the medium temperature range (600 ÷ 800 K) due to the crystal structure features [14-18]. It is known, that one of the effective ways to optimize the properties of functional materials is to obtain solid solutions based on them. For this purpose, it is advisable to study phase equilibria in the corresponding systems [19-24]. Earlier, in some previous works [25-33] we studied a few systems based on copper chalcogenides, in which we found new phases of variable compositions. In this paper we present new experimental data of studying of phase equilibria in the Cu_2Se-Cu_2SnSe_3-Cu_3SbSe_4 subsystem of the Cu-Sn-Sb-Se system.

The initial compound Cu_2Se melts congruently at 1403 K and has a polymorphous transformation at 396 K [34]. The homogeneity region of this compound is located at compositions enriched with selenium and has maximal value at 800 K (33.3-36.6 at% Se). The high-temperature modification of Cu_2Se crystallizes in a cubic structure with the lattice parameters: (Sp. gr. Fm3m), a=5.859(1) Å. The low-modification has monocline structure (Sp. gr. *C*2/*c*) with the unit cell parameters: a=7.1379(4) Å, b=12.3823(7) Å, c=27.3904(9) Å and β=94.308^0 [35].

Cu_3SbSe_4 melts congruently at 755 K and crystallizes in a tetragonal structure (Sp. gr. *I42m*) with lattice parameters: a=b=5.6609(8) Å; c=11.280(5) Å [36]. Copper-tin selenide Cu_2SnSe_3 melts congruently at 968 K and has a polymorphic transition at 948 K [37,38]. The high-temperature modification crystallizes in a

cubic lattice (a=5.6877) [39, 40] and low-temperature one is monocline (space group *Cc*) with the unit cell parameters: a =6.9670(3) Å, b=12.0493(7) Å, c=6.9453(3) Å, β=109.19(1)°; z=4 [39, 40].

The phase diagram of the Cu_2SnSe_3-Cu_3SbSe_4 system were studied in [41], based on the results of DTA and X-ray diffraction analysis. The Cu_2SnSe_3-Cu_3SbSe_4 section is quasi-binary and has phase diagram with eutectic type (coordinates: 68 mol% Cu_3SbSe_4, 727 K) and formation of wide regions of solid solutions (α- and β-phases) based on both starting compounds. According to [42], the Cu_3SbSe_4-Cu_2Se system is a quasi-binary, and the solubility area (not more than 5 mol %) based on initial compounds is observed. The Cu_2Se-Cu_2SnSe_3 section has the phase diagram of the simple eutectic type. Eutectic point has coordinates 938 K and ~55 mol% Cu_2Se [43].

2. Experimental part

2.1. Synthesis

Stoichiometric amounts of high purity elemental substances from EVOCHEM ADVANCED MATERIALS GMBH (Germany), copper granules (Cu-00029, 999999%), antimony granules (Sb-00005, 99.999%) and selenium granules (Se-00002, 99.999%) were used for synthesis. Cu_2Se, Cu_3SbSe_4 and Cu_2SnSe_3 were synthesized by fusion of simple components in evacuated to ~10^{-2} Pa and sealed quartz ampoules at temperatures 50 ºC above from the melting points of the synthesized compounds.

Cu_2Se was produced in a two-zone inclined furnace. The temperature of the lower,"hot" zone was 1300 K, while the upper "cold", zone was 900 K that is somewhat below the selenium boiling temperature (958 K [44]). In order to obtain homogeneous Cu_2Se, the ampoule with the stoichiometric composition, was quenched from a temperature of 1300 K in cold water after synthesis [45]. The ternary compounds Cu_2SnSe_3 and Cu_3SbSe_4 were synthesized in single-zone mode at temperatures of 1000 and 850 K, respectively, and then annealed at 700 K for 50 hours.

All of the synthesized compounds were controlled using differential thermal analysis (DTA) and X-ray diffraction (XRD). The melting points of all synthesized compounds were close to literature data within an error of ±3 K. More than 30 alloys of the Cu_2Se-Cu_3SbSe_4-Cu_2SnSe_3 system were prepared.

From the DTA data for selected compositions of cast non-homogenized alloys, it was indicated that their crystallization was completed higher than 650 K. Therefore, to achieve a state closer to the equilibrium, alloys were annealed at 600 K within 500-700 h.

2.2. Research Methods

The alloys of the studied system were characterized by DTA, X-ray diffraction and SEM methods. DTA measurements were conducted using Netzsch 404 F1 Pegasus system and the NETZSCH Proteus software with a heating rate of 10 K min-1 and accuracy was within ±2 K.

The X-ray analysis was carried out at room temperature by the D8 advance powder diffractometer with $CuK\alpha_1$ radiation from Bruker, and patterns were indexed using the Topas V3.0 software.

The SEM studies were carried out in back scattered to reveal the compositional contrast between different phases. For this purpose, SEM analysis of some polished samples was performed using a TESCAN Vega 3 SBH scanning electron microscope and a Thermo Scientific Ultra Dry Compact EDS detector.

3. Results and discussion

3.1. Isothermal section of the phase diagram at 600 K.

Fig. 1 shows a diagram of the solid phase equilibria established on the basis of the results of XRD and SEM of annealed at 600 K samples of the Cu_2Se-Cu_2SnSe_3-Cu_3SbSe_4 system. It can be seen from the Fig. 1, the system is characterized by the formation of wide region of solid solution based on the initial components. Area of solid solutions based on HT-Cu_2Se are

5-6 mol%. Homogeneity areas of α- and β- solid solutions formed along the Cu_2SnSe_3-Cu_3SbSe_4 section penetrate into the 3-8 mol % of concentration triangle and the corresponding single-phase bands are formed. (HT-Cu_2Se), α- and β- phases with each other produce three two-phase: (HT-Cu_2Se) + α, (HT-Cu_2Se) + β, α + β areas and one three-phase (HT-Cu_2Se) + α + β area. All phase areas were confirmed by XRD and SEM technique.

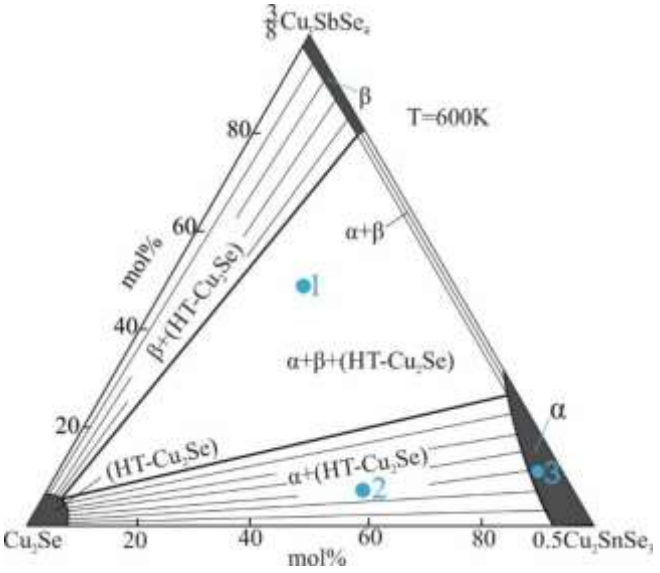

Fig.1. Diagram of solid-phase equilibria in the Cu_2Se-Cu_3SbSe_4 -Cu_2SnSe_3 at the 600 K

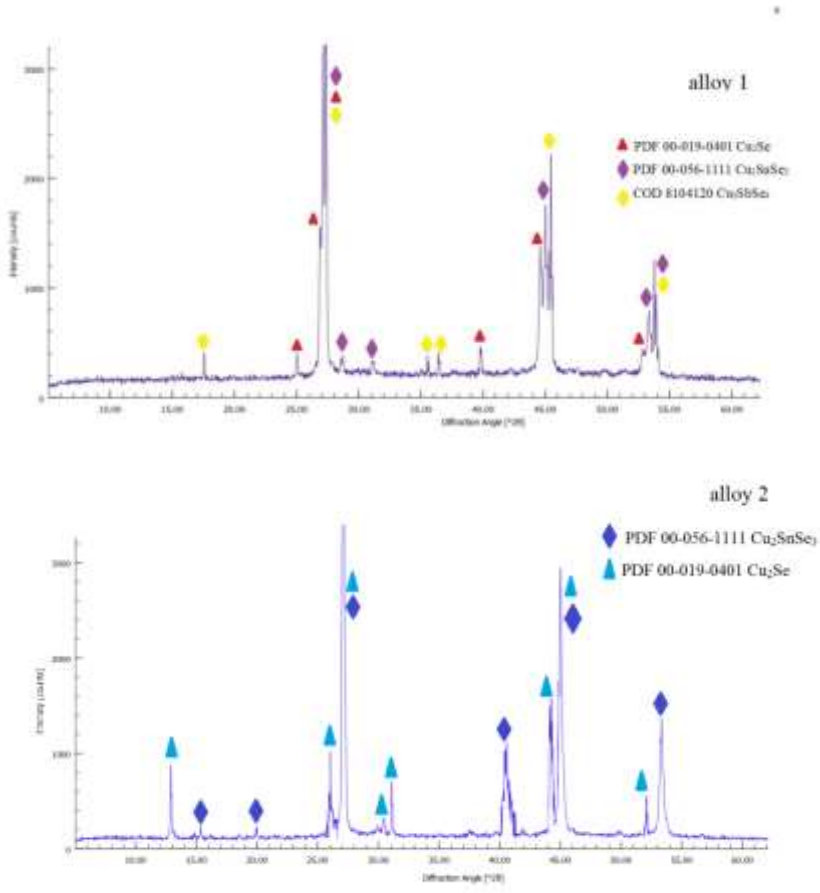

Fig.2. X-ray powder diffraction patterns of the alloy 1 (30%Cu_2Se-30%Cu_2SnSe_3-40%Cu_3SbSe_4) and alloy 2 (40% Cu_2Se-60Cu_2SnSe_3).

Powder diffraction patterns of alloys were confirmed by X-ray phase analyses. It can be seen from Fig.2 the diffraction patterns of the selected alloy #1 (see Fig.1) consist of the three-phase mixture α +β +(HT-Cu_2Se), and alloy #2 comprises the two-phase mixture of α+(HT-Cu_2Se).

SEM–EDS analysis of certain composition of the α-phase showed their single-phase character. For example, Figure 3 shows the SEM image of the α-phase with the composition 10 mol% Cu_3SbSe_4 (alloy 3 in Fig.1). The element composition of the alloy is shown in Table 1 using results of the EDS analysis and corresponds to the formula $Cu_{2.1}Sb_{0.1}Sn_{0.9}Se_{3.1}$ (Fig.4).

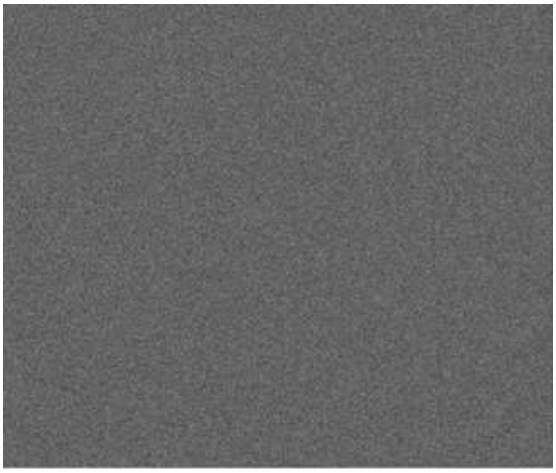

Fig.3. SEM image of α-phase with composition $Cu_{2.1}Sb_{0.1}Sn_{0.9}Se_3$

Table 1. Elemental analysis results for $Cu_{2.1}Sb_{0.1}Sn_{0.9}Se_3$.

Element	Weight %	Atomic %
Cu *K*	25,2	33,87
Sb *K*	3,1	1,62
Sn *L*	22,0	14,51
Se *L*	49,7	50
Total	**100,0**	**100,0**

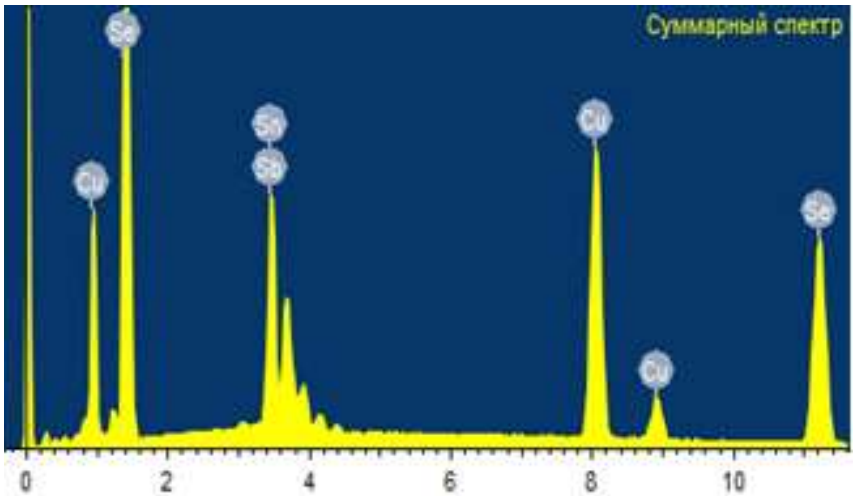

Fig.4. EDS analysis for the $Cu_{2.1}Sb_{0.1}Sn_{0.9}Se_3$

3.2. Liquidus surfase

The projection of the liquidus surface of the Cu_2Se-Cu_3SbSe_4-Cu_2SnSe_3 system was established using our experimental results and literature data for boundary quasibinary systems [41-43] (Fig. 5). As can be seen, the considered plane of the Cu-Sn-Sb-Se concentration tetrahedron is a quası-ternary system and its T-x-y phase diagram belongs to the eutectic type.

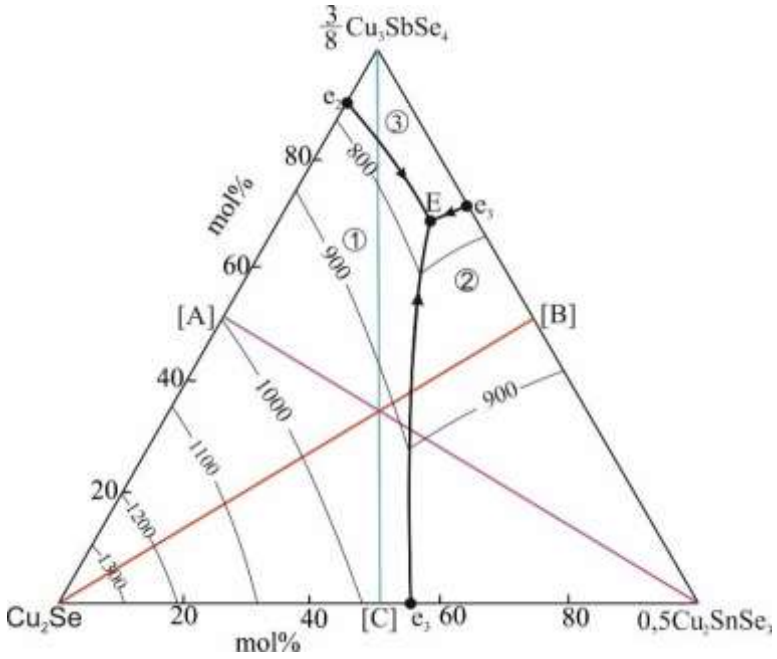

Fig. 5. Liquidus surfase of the Cu_2Se- Cu_3SbSe_4-Cu_2SnSe_3 system.Primary crystallization fields: 1-HT-Cu_2Se; 2-α-; 3- β-phase

The liquidus surface of the Cu_2Se-Cu_2SnSe_3-Cu_3SbSe_4 system consists of three fields of primary crystallization of (HT-Cu2Se), α- and β- phases. The curves from the eutectic points of boundary quasibinary systems (e_1E, e_2E, e_3E) intersect in the triple eutectic point. These curves are characterized by the following monovariant eutectic equilibria:

$$L \leftrightarrow (\text{HT-Cu2Se}) + \alpha \qquad (e_1E;, 940\text{-}725\ K) \qquad (1)$$
$$L \leftrightarrow (\text{HT-Cu2Se}) + \beta \qquad (e_2E; 750\text{-}725\ K) \qquad (2)$$
$$L \leftrightarrow \alpha + \beta \qquad (e_3E; 733\text{-}725\ K) \qquad (3)$$

The following nonvariant equilibrium is formed at the triple eutectic point E (725 K):

$$L \leftrightarrow (\text{HT-}Cu_2Se) + \alpha + \beta \qquad (4)$$

Some polythermal sections of the phase diagram were constructed in order to observe the crystallization processes and specify the boundaries of the liquidus areas in the system.

3.3. Polythermal sections of the phase diagram

Phase equilibria of three polythermal sections of the T-x-y diagram of the Cu_2Se-Cu_3SbSe_4-Cu_2SnSe_3 system were plotted and briefly interpreted.

The Cu_2Se - [B] section (where [B] is an alloy of the $3/8Cu_3SbSe_4$-$0{,}5Cu_2SnSe_3$ side system corresponding to the composition 1:1). The liquidus of this section consists of 2 curves (Fig.6). Solid solution based on HT-Cu_2Se and α-phase based on Cu_2SnSe_3 are initially crystallized from the melt (from left to right).

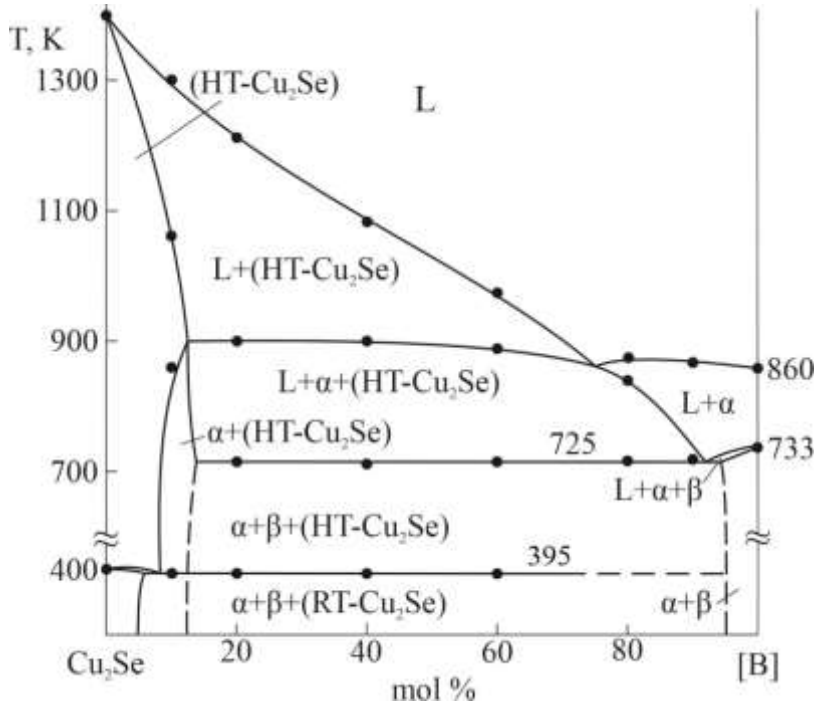

Fig. 6. Phase diagram of the Cu_2Se-[B]. [B] – alloy of the $0{,}5Cu_2SnSe_3$-$3/8Cu_3SbSe_4$ side system coesponding to the composition 1:1

At the intersection point of these two curves, the eutectic mixture (HT-Cu_2Se) + α crystallizes directly from the melt. Below the liquidus, monovariant process (1) continues in a wide region (~13-75 mol%). A monovariant crystallization process is proceeds according the reaction (3) in a small composition (~ >90 mol%) range. Then the crystallization process is completed by the nonvariant eutectic reaction (4).

It should be noted that crystallization process near the Cu_2Se is finished by the precipitation of the (HT-Cu_2Se) phase. As the temperature decreases, α-phase is released from this phase and two-phase region (HT-Cu_2Se) + α is formed. Near the [B] point (> 95 mol%), the process ends according to reaction (3) and two-phase region α+β is formed in the subsolidus.

The formation of solid solution on the basis of Cu_2Se is accompanied by a decrease in the polymorphic transformation temperature (400 K) of this compound and the emergence of eutectoid equilibrium (395 K).

The [A]- $0{,}5Cu_2SnSe_3$ section. This section of the phase diagram is presented in Fig.7 (where [A] is an alloy of the Cu_2Se – $3/8Cu_3SbSe_4$ side system corresponding to the composition 1:1).

The liquidus of this section consists of two curves reflecting the primary crystallization of (HT-Cu_2Se) and α-phases. Below the liquidus, from left to right, crystallization continues in accordance with monovariant schemes (2) and (1). Three-phase fields L+ (HT-Cu_2Se) +β (0-20 mol%) and L + (HT-Cu_2Se) +α (20-85 mol %) are formed in the system during the process. Then the crystallization of samples in the range of 25-70 mol% is completed with a nonvariant eutectic reaction (4). In the range of composition 0-15 mol% Cu_2SnSe_3, crystallization is completed according to the reaction (2) and two-phase field (HT-Cu_2Se) + β is formed in subsolidus. In the ~70 - 85 mol% $0/.5Cu_2SnSe_3$, the crystallization is completed by reaction (1) which leads to the formation of α + (HT-Cu_2Se) in the subsolidus. Finally, the crystallization in the system completes near the Cu_2SnSe_3 and resulted by the formation of α-solid solutions.

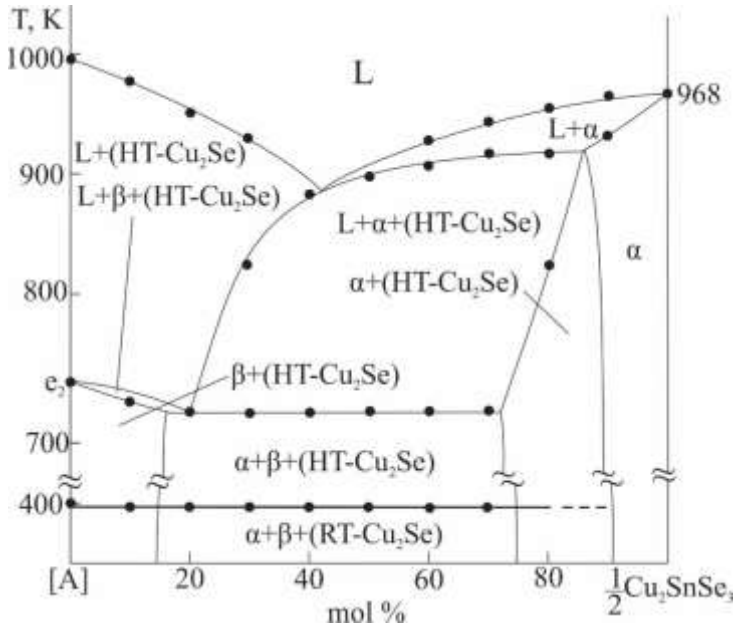

Fig. 7. Phase diagram of the [A]- $1/2Cu_2SnSe_3$ system. [A] – alloy of the Cu_2Se-$3/8Cu_3SbSe_4$ side system corresponding to the composition 1:1

The horizontal line at 395 K represents the polymorphic transition of (HT-Cu_2Se) ↔ (RT-Cu_2Se), as in the previous section.

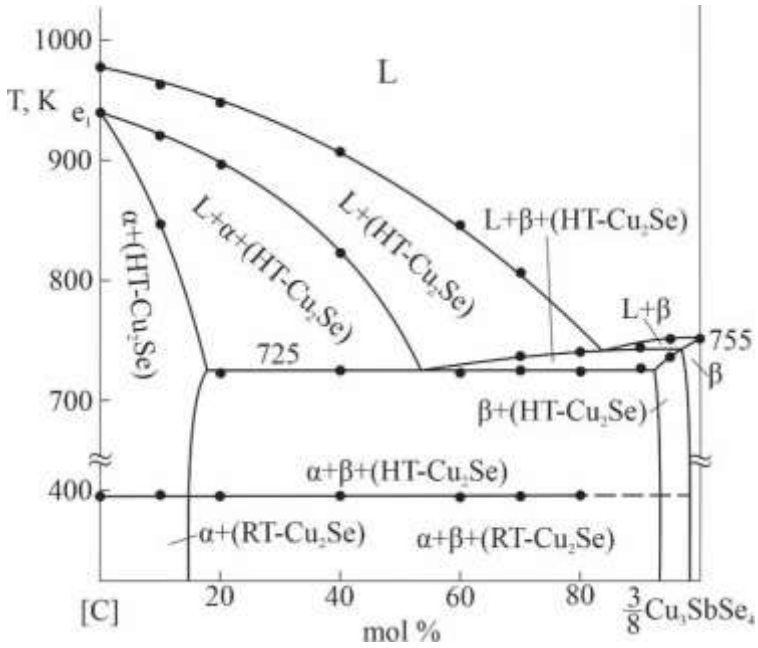

Fig. 8. Phase diagram of the [C]- $3/8Cu_3SbSe_4$. [C] – alloy of the Cu_2Se–$0.5Cu_2SnSe_3$ side system corresponding to the composition 1:1

Section [C] - $3/8Cu_3SbSe_4$ (Fig. 8) (where [C] is an alloy of the Cu_2Se-$0{,}5Cu_2SnSe_3$ side system corresponding to the composition 1:1). First of all (HT-Cu_2Se) crystallizes from liquid in a wide range of composition (0-85 mol%), while, in the range of >85 mol% β-phase crystallizes and the afterwards corresponding two-phase region is formed. The crystallization process continues according to reaction (1) in the of 0-55 mol% composition range and in accordance with reaction (2) in the 55-95 mol% area. As a consequence of these processes two

three-phase fields L + α + (HT-Cu_2Se) and L + β + (HT-Cu_2Se) are formed. It should be noted that, the completion of reaction (1) ends with consumption of the liquid phase in the of 0-18 mol% concentration area and the α+ (HT-Cu_2Se) two-phase region is formed. Near the Cu_3SbSe_4, the processing of crystallization is completed by L↔β or L ↔ β + (HT-Cu_2Se) equilibrium, thus, β and β + (HT-Cu_2Se) fields are formed in the subsolidus. The process of crystallization of the samples in the composition range of ~18-93 mol% completes by a nonvariant eutectic reaction (4) and tree-phase region α + β + (HT-Cu_2Se) is formed in the subsolidus, which transforms into α + β + (RT-Cu_2Se), at 395 K.

Conclusion

The complete picture of phase equilibria in the quasi-ternary system Cu_2Se-Cu_2SnSe_3-Cu_3SbSe_4 was obtained, including the solid-phase equilibria of the system at 600 K, a series of polythermal section and the projection of liquidus surface, based on the experimental data. The liquidus surface consists of 3 areas related to the primary crystallization of (HT-Cu_2Se), α- and β- phase based on the Cu_2SnSe_3 and Cu_3SbSe_4. The studied qausi-ternary system is characterized by the formation of limited regions of solid solution based on the initial compounds. Homogeneity regions of α- and β-solid solutions which were formed on the boundary section (Cu_2SnSe_3-Cu_3SbSe_4) penetrate into the 3-8 mol% concentration triangle and forming single-phase bands.

Acknowledgment

This work supported by the Azerbaijan Science Foundation – **Grant No AEF-MCG-2022-1(42)-12/10/4-M-10**.

Referenses

1. Wei T.R., Qin Y., Deng T., Song Q., Jiang B., Liu R., Chen L. Copper chalcogenide thermoelectric materials. *Science China Materials*. 2018, Vol. **62**, p. 8–24. https://doi.org/10.1007/ s40843-018-9314-5
2. Powell A.V. Recent developments in Earth-abundant copper-sulfide thermoelectric materials. *Journal of Applied Physics*, 2019, Vol.**126(10)**, 100901p. https://doi.org/10.1063/1.5119345
3. Alonso-Vante N. Chalcogenide materials for energy conversion. Pathways to oxygen and hydrogen reactions. *Springer Cham*, 2018, 226 p. https://doi. org/10.1007/978-3-319-89612-0
4. Applications of Chalcogenides: S, Se, and Te. Ahluwalia G. K. (ed.). *Cham. Springer*, 2016, 461 p. https://doi.org/10.1007/978-3-319-41190-3
5. Peccerillo E. and Ken D. Copper–antimony and copper–bismuth chalcogenides—Research opportunities and review for solar photovoltaics. *Materials Research Society*, 2018, Vol. **5**, 9 doi:10.1557/mre.2018.10
6. Sanghoon X.L., Tengfei L.J., Zhang L.Y.-H. Chalcogenide. From 3D to 2D and beyond. *Elsevier*, 2019, 398 p.
7. Huiying Fu.J. Environmentally friendly and earth-abundant colloidal chalcogenide nanocrystals for photovoltaic applications. *Mater. Chem. C.* 2018, Vol. **6**, p. 414–445
8. Mikuła A., Mars K., Nieroda P., Rutkowski P. Copper chalcogenide-copper tetrahedrite composites – a new concept for stable thermoelectric materials dased on the chalcogenide system. *Materials*, 2021, Vol. **14(10)**, 2635.doi: 10.3390/ma14102635.
9. Palchoudhury S., Ramasamy K., Gupta A., Multinary Copper-based Chalcogenide Nanocrystal Systems from the Perspective of Device Applications. *Nanoscale Advances*, 2020, Vol. **2**, p. 3069-3082. doi:10.1039/D0NA00399A
10. Tippireddy S., Prem Kumar D.S., Karati A., Mallik R.C. Effect of Sn substitution on the thermoelectric properties of synthetic tetrahedrite. *ACS Applied Materials and Interfaces*. 2019, Vol. **116(24)**, p. 21686–

21696. https://doi.org/10.1021/acsami.9b02956
11. Yang J., Lu B., Song R., Hou H., Zhao L., Zhang X., Liu G., Qiao G. Realizing enhanced thermoelectric properties in Cu_2GeSe_3 via a synergistic effect of In and Ag dual-doping. *Journal of the European Ceramic Society*. 2022, Vol. **42**, p. 169–174.
12. Sun F.H., Dong J., Dey S., Li J.F. Enhanced thermoelectric performance of $Cu_{12}Sb_4S_{13}$−d tetrahedrite via nickel doping. *Science China Materials*, 2018, Vol. **61(9)**, p. 1209–1217. https://doi.org/10.1007/s40843-018-9241-x
13. Liu M., Qin X., Liu C. Substitution site selection and thermoelectric performance-enhancing mechanism of $Cu_{12}Sb_4S_{13}$ doped with Pb/Ge/Sn. *Physica Status Solidi B*. 2022, Vol. **259**, p. 2100275–2100278. https:// doi.org/10.1002/pssb.202100275
14. Prasad K.S., Rao A., Chauhan N.S., Bhardwaj R. Thermoelectric properties of p-type Sb-doped Cu_2SnSe_3 near room and mid temperature applications. *Appl. Phys. A.* 2018, Vol. **124**, 98.
15. Kim F.S., Suekuni K., Nishiate H., Ohta M., Tanaka H.I., Takabatake T. Tuning the charge carrier density in the thermoelectric colusite. *J. Appl. Phys*. 2016, Vol. **119**, 175105 p.
16. Suekun K., Takabatake T. Research update: Cu–S based synthetic minerals as efficient thermoelectric materials at medium temperatures. *Apl. Mater*. 2016, Vol. **4**, 104503 p.
17. Min L., Ying P., Li X., Cui J. Regulation of both the crystal structure and carrier concentration leading to the improved thermoelectric performance of Cu_3SbSe4-based chalcogenides. *J. Phys. D: Appl. Phys*. 2020, Vol. **53(7)**, 075304 p.
18. Moorthy M., Srinivasan B., Berthebaud D., Parasuraman R., Althaf R., Perumal S. Enhanced thermoelectric performance and mechanical property in layered chalcostibite $CuSb_{1-x}Pb_xSe_2$. *ACS Applied Energy Materials*. 2023, Vol. **6(2)**, p. 723-733
19. Babanly M.B., Chulkov E.V., Aliev Z.S., Shevelkov A.V., Amiraslanov I. R. Phase diagrams in materials science of topological insulators based on metal chalkogenides. *Russ. J. Inorg. Chem.* 2017, Vol. **62(13),** p. 1703–1729.
20. Imamaliyeva S.Z. Phase diagrams in the development of thallium-REE tellurides with Tl5Te3 structure and multicomponent phases based on them. *Kondensirovannye Sredy I Mezhfaznye Granitsy = Condensed Matter and Interphases,* 2018, Vol. **20(3)**, p. 332-347. DOI: https://doi.org/10.17308/kcmf.2018.20/570
21. Mammadov F.M., Babanly D.M., Amiraslanov I.R., Tagiyev D.B., Babanly M.B. FeS–Ga_2S_3–In_2S_3 System. *Russ. J. Inorg. Chem*. 2021. Vol. **66(10)**, p. 1533-1543. https://doi.org/10.1134/S0036023621100090
22. Babanly M.B., Mashadiyeva L.F., Imamaliyeva S.Z., Tagiev D.B., Babanly D.M., Yusibov Yu.A. Thermodynamic properties of complex copper chalcogenides (Review). *Chemical Problems*, 2024, Vol. 22(3), p. 243-280. https://doi.org/10.32737/2221-8688-2024-3-243-280
23. Mammadov F.M., Imamaliyeva S.Z., Jafarov Ya.I., Bakhtiyarly I.B., Babanly M.B. Phase equilibria in the MnTe–$MnGa_2Te_4$–$MnIn_2Te_4$ system. *Condensed Matter and Interphases*. 2022, Vol. **24(3)**, p. 335–344. https://doi.org/10.17308/kcmf.2022.24/9856
24. Mammadov F.M., Amiraslanov I.R., Aliyeva Y.R., Ragimov S.SL., Mashadiyeva L.F., Babanly M.B. Phase equilibria in the $MnGa_2Te_4$-$MnIn_2Te_4$ system, crystal structure and physical properties of $MnGaInTe_4$. *Acta Chim. Slov*. 2019, Vol. **66**, p. 466-472. https://doi.org/10.17344/acsi.2019.4988
25. Ismayilova E.N., Mashadieva L.F., Bakhtiyarly I.B., Babanly M.B. Phase equilibria in the Cu_2Se–SnSe–$CuSbSe_2$ system. *Russian Journal of Inorganic Chemistry*. 2019, Vol. **64(6)**, p. 801–809. https://doi. org/10.1134/S0036023619060093

26. Ismayilova E.N., Baladzhayeva A.N., Mashadiyeva L.F. Phase equilibria along the Cu_3SbSe_4-$GeSe_2$ section of The Cu-Ge-Sb-Se. *New Materials, Compounds and Applications*. 2021, Vol. **5(1)**, p. 52–58.
27. Ismayilova E.N., Mashadiyeva L.F., Bakhtiyarly I.B., Babanly M.B. Phase equilibria in the Cu_2Se-SnSe-Sb_2Se_3 system. *Azerbaijan Chemical Journal*, 2022, No. **1**, p. 73–82. https://doi.org/10.32737/0005- 2531-2022-1-73-82
28. Ismayilova E.N., Mashadiyeva L.F., Bakhtiyarly I.B., Babanly M.B. Phase equilibria in the Cu_2SnSe_3–Sb_2Se_3–Se system. *Condensed Matter and Interphases*. 2023, Vol. **25(1)**, p. 47–54
29. Mashadiyeva L.F., Babanly D.M., Hasanova Z.T., Yusibov Y.A., Babanly M.B. Phase Relations in the Cu-As-S System and Thermodynamic Properties of Copper-Arsenic Sulfides. *J. Phase Equilib. Diffus*, 2024, Vol. **45**, p. 567-582. https://doi.org/10.1007/s11669-024-01115-w
30. Bayramova U.R., Babanly K.N., Ahmadov E.I., Mashadiyeva L.F., Babanly M.B. Phase Equilibria in the Cu_2S-Cu_8SiS_6-Cu_8GeS_6 System and Thermodynamic Functions of Phase Transitions of the $Cu_8Si_{(1-X)}Ge_XS_6$ Argyrodite Phases. *J. Phase Equilib. Diffus*. 2023, Vol. **44** p. 509–519. https://doi.org/10.1007/s11669-023-01054-y
31. Bairamova U.R., Babanly K.N., Mashadieva L.F., Yusibov Yu.A., Babanly M.B. Phase Equilibria in the Cu_2Se–Cu_8SiSe_6–Cu_8GeSe_6 System. *Russ. J. Inorg. Chem*. 2023, Vol. **68**, p. 1611–1621. https://doi.org/10.1134/S0036023623602027
32. Mashadiyeva L.F., Babanly D.M., Poladova A.N., Yusibov Y.A., Babanly M.B. Liquidus surface and phase relations in the Cu-Sb-S system. Properties and Uses of Antimony – Editor: David J. Jenkins, *Nova Science Publishers*, 2022, p. 45-72. https://doi.org/10.52305/OJKB5395
33. Mashadieva L.F., Alieva Z.M., Mirzoeva R.Dzh., Yusibov Yu.A., Shevel'kov A.V., Babanly M.B. Phase Equilibria in the Cu_2Se–$GeSe_2$ –$SnSe_2$ System. *Russian Journal of Inorganic Chemistry*, 2022, Vol. **67(5)**, p. 670–682. https://doi.org/10.1134/S0036023622050126
34. Binary Alloy Phase Diagrams. Ed. Massalski T.B. Second ed., *ASM International, Materials Park*, Ohio, 1990. P. 3589.
35. Gulay L., Daszkiewicz M., Strok O., Pietraszko A. Crystal structure of Cu_2Se. *Chem. Met. Alloys*. 2011, Vol. **4**. p. 200–205.
36. Pfitzner A. Crystal structure of tricopper tetraselenoantimonate Cu_3SbSe_4. *Zeitschrift für Kristallographie-Crystalline Materials*,1994, Vol. **209(8)**, p. 685-685
37. Parasyuk O.V., Olekseyuk I.D., Marchuk O.V. The Cu_2Se–HgSe–$SnSe_2$ system. *Journal of Alloys and Compounds*. 1999, Vol. **287(1-2)**, p. 197–205. https://doi.org/10.1016/S0925-8388(99)00047-X
38. Babanly M.B., Yusibov Yu.A., Abishov V.T. Three-component chalcogenides based on copper and silver. *Baku: BSU Publ*., 1993, 342 p. (In Russ.).
39. Delgado G.E., Mora A.J., Marcano G., Rincon C. Crystal structure refinement of the semiconducting compound Cu_2SnSe_3 from X-ray powder diffraction data. *Materials Research Bulletin*. 2003, Vol. **38**, p. 1949–1955. https://doi.org/10.1016/j.materresbull.2003.09.017
40. Marcano G., Chalbaud L., Rincón C., Sánchez P.G. Crystal growth and structure of the semiconductor Cu_2SnSe_3. *Materials Letters*. 2002, Vol. **53(3)**, p. 151–154. https://doi.org/10.1016/s0167-577x(01)00466-9
41. Исмаилова Э.Н. Фазовая диаграмма системы Cu_2SnSe_3-Cu_3SbSe_4. *Sumqayıt Dövlət Universiteti – "Elmi Xəbərlər"– Təbiət və texniki elmlər bölməsi*, 2022, Vol. **22(3)**, DOI 10.54758/16801245_2022_22_3_33
42. Chorba O.J., Sabov M.Yu., Filep M.J., Pogodin A.I. Phase Equilibria In The Section Cu_2Se – Cu_3SbSe_4. *Scientific Bulletin of the Uzhhorod University Series*

«Chemistry», 2023, Vol. **49(1)**, p. 20-24. DOI:10.24144/2414-0260.2023.1.20-24

43. Климович О.С., Іващенко І.А., Олексеюк І.Д., Змій О.Ф. Фазові Рівноваги У Квазіпотрійній Системі Cu_2Se – $SnSe_2$ – As_2Se_3. *Вісник ОНУ. Хімія*. 2020, Том. **25(1(73))**, p. 31-42
44. Emsli Dzh. Elementy. M.: *Mir*, 1993. P. 256.
45. Glazov V.M., Burkhanov A.S., Saleyeva N.M. K metodike polucheniya odnofaznykh khalkogenidov medi i serebra. *Izv. AN SSSR. Neorgan. materialy*. 1977, T. **13(5)**. C. 917–919.